Article

Journal of the Brazilian Chemical Society

https://dx.doi.org/10.21577/0103-5053.20240052

J. Braz. Chem. Soc. **2024**, *35*, 9, e-20240052, 1-9

Radioinduced Modulatory Response of Lipid Profiles of Wistar Rats Brain Monitored by DESI-MS Imaging

Matheus F. S. Mingote,[a] Camila Cristina A. de Paula,[b] Tarcísio P. R. de Campos,[a] Géssica Adriana Vasconcelos,[c] Boniek G. Vaz[c] and Rodinei Augusti[*,b]*

[a]*Departamento de Energia Nuclear, Universidade Federal de Minas Gerais, 31270-901 Belo Horizonte-MG, Brazil*

[b]*Departamento de Química, Universidade Federal de Minas Gerais, 31270-901 Belo Horizonte-MG, Brazil*

[c]*Instituto de Química, Universidade Federal de Goiás, 74690-900 Goiânia-GO, Brazil*

The ionizing radiation used in radiotherapy can break down deoxyribonucleic acid bonds, generate reactive oxygen and nitrogen species, alter intracellular proteins, and induce changes in the lipidome. This study delves into examining lipid classes and their spatial distribution in the brains of Wistar rats exposed to ionizing radiation. Healthy male isogenic Wistar rats (n = 15) were divided into a control group (CG, n = 3) and an irradiated group (IRG, n = 12). The individuals of the IRG group were subjected to total body irradiation (TBI) using a Co-60 source and a radiation dose of 5 Gy. The IRG group was subdivided into four subgroups corresponding to 168, 96, 48, and 24 h before sacrifice. The brains were sliced into the sagittal direction, and the slices were analyzed using the desorption electrospray ionization mass spectrometry imaging (DESI-MSI) approach. The mass spectrometry results and information from the Metabolite and Chemical Entity Database (METLINTM) and Lipid Metabolites and Pathways Strategy (LIPID MAPS) databases enabled the identification of lipids belonging to distinct classes. The DESI-MS images revealed distinctive spatial distributions of these lipids and the modulatory response induced by the radiation over time.

Keywords: desorption electrospray ionization (DESI), mass spectrometry imaging, total body irradiation (TBI), Wistar rat's brain lipid profile, spatial distribution of lipids, modulatory response

Introduction

Tumors in the central nervous system (CNS) are highly malignant and have a strong tendency to progress, causing harmful effects that can result in significant neurological changes. Oncological radiotherapy, a specialized treatment, uses ionizing radiation to cure or control the growth of these neoplasms. However, this form of radiation affects both tumor cells and surrounding healthy cells, often leading to neurotoxicity and significant neurocognitive disorders.[1,2] In radiotherapy, ionizing radiation is employed to decrease the clonogenicity of neoplasms (both malignant and benign) through careful planning and the prescription of effective therapeutic doses.[3] The resulting radio-induced toxicities can manifest as leukoencephalopathies, characterized by extensive white matter lesions and lacunar infarcts, leading to neurocognitive decline and decreased life quality.[4] Higher radiation doses can exacerbate effects such as fatigue, erythema, alopecia, headache, nausea, vomiting, dry mouth, conjunctivitis, neuropathies, and neuritis. Additionally, there is a risk of more severe consequences such as ototoxicity, retinopathies, blindness, cataracts, and hypothalamic-pituitary dysfunctions. The cognitive deficits observed may significantly impair intellectual development, as measured by the Full-Scale Intelligence Quotient (FSIQ).[5]

Ionizing radiation induces deoxyribonucleic acid (DNA) damage directly and indirectly by promoting the formation of reactive oxygen (ROS) and nitrogen (RNS) species. ROS and RNS pose a significant threat as they contribute to genomic damage. Direct ionization events lead to alterations and deletions in DNA bases, disruption of hydrogen bonds, and the fragmentation of single-strand breaks (SSBs) or double-strand breaks (DSBs). ROS

*e-mail: augusti.rodinei@gmail.com
Editor handled this article: Ivo M. Raimundo Jr. (Associate)

initiates lipoperoxidation in polyunsaturated fatty acids, generating highly reactive by-products such as aldehydes, ketones, epoxides, and hydrocarbons. This process results in mutations and genetic damage.[6] Lipid peroxidation is a cytotoxic event characterized by successive biochemical reactions activated by free radicals, leading to extensive oxidation of unsaturated fatty acids and membranes. The by-products formed bring about structural and functional changes in the cell membrane, impacting the flow of ionic and molecular substrates.[7] For instance, the peroxidation of esterified arachidonic acid, a constituent of the cell membrane, predominantly promotes the formation of isoprostanes, resulting in critical physicochemical alterations that affect the fluidity of the membrane and deactivate enzymatic transmembrane receptors responsible for intracellular and nuclear signaling.[8]

Lipidomics entails identifying and quantifying lipids, assessing their interactions with other biomolecules and metabolites, and allowing for structural evaluation and understanding of intracellular morphophysiology and its response to various disorders within the system. Lipidomics broadens the knowledge of the mechanisms that drive alterations in cellular functioning by examining spatial and temporal changes in the content and composition of different lipids (including membrane and neurotransmission ones) under various physiological or pathological states. Elucidating these mechanisms helps understand specific pathophysiological processes, particularly those involved in neurodegenerative diseases.[9-13]

Desorption electrospray ionization mass spectrometry imaging (DESI-MSI) was employed to access the lipid profiles of various animal tissues, aiming to identify disease markers and comprehend the metabolic roles of different lipids in the body.[14-22] These images display the spatial distribution of ion signals through a color scale, reflecting the intensity observed in the mass spectra. In DESI-MSI, the mass spectra are acquired by scanning the entire surface at each x/y coordinate, with ion intensities being converted into images. In summary, for this technique, a high voltage is applied to a capillary containing a polar solvent. The solvent, propelled from the capillary by an inert nebulizer gas, reaches the sample surface at an appropriate angle, transferring charge to ionizable species. The generated ions then enter the mass spectrometer, and their mass-to-charge ratios (*m/z*) are determined.[14]

The present study employs the DESI-MSI technique to examine the changes in the spatial distribution of lipids in Wistar rat brains before and after gamma radiation exposure. This is the first report that evaluates a possible modulation of lipid profiles resulting from radiation exposure.

Experimental

Animals

Fifteen (n = 15) healthy Wistar rats aged 11 weeks and with body weight between 300 ± 15 g were selected. The animals were divided into two groups: a control group (n = 3, CG) and another subjected to total body irradiation (TBI), called the irradiated group (n = 12, IRG), subdivided into 4 subgroups containing 3 animals, each. The animals were submitted to the same photographic (day/night) period of 12 h with free access to food and water. The Central Biturium, a Federal University of Minas Gerais facility, provided animals of the same lineage and family. The animal experiments took place with the approval of the Animal Experimentation Ethics Committee of the Federal University of Minas Gerais, approved process 339/2014.

Irradiation protocol

Each subgroup of IRG animals was placed in appropriate boxes and subjected to total body irradiation (TBI) by exposure to the Co-60 source (absorbed dose of 5 Gy) at the Gamma Irradiation Laboratory, Nuclear Energy Development Center of the Federal University of Minas Gerais. The following irradiation parameters were employed: activity of the animals on the irradiation date (26,940.00 Ci); chimney distance (1.6 m); current dose rate (87.91 Gy h^{-1}); applied dose (5 Gy); exposure time (205 min). Such parameters were defined based on previous experience of our research group. The procedure was carried out at 10:00 am of each day.

Tissue preparation

The animals belonging to each subgroup were sacrificed on the same date to remove the brains. Therefore, each subgroup was exposed to the same radiation conditions before the sacrifice date to perform the post-radiation kinetic study. Each subgroup was submitted to the radiation protocol above described and was sacrificed after 168, 96, 48, and 24 h, totaling four subgroups. The animals were anesthetized by intramuscular injection to remove the organs using 5% ketamine (0.2 mL for each 100 g of body weight) and 2% m v^{-1} xylazine (0.1 mL for each 100 g of body weight). After sacrificing and removing the brain, the organs were weighed, stored in duly identified plastic bags, and instantly frozen in a mixture of dry ice and *n*-heptane at approximately −78 °C to avoid denaturation. The organs were then stored in a

freezer (at −80 °C) until the brain slices preparation in the cryostat. The organs were removed from the freezer to reach the cryostat (Leica CM3050-S) temperature (−30° C) before cutting. The brains were sectioned in the sagittal direction with a slide thickness of 14 µm. The slides were then returned to the freezer at −80 ºC for further analysis by DESI-MSI.

Desorption electrospray mass spectrometry (DESI)

Before analysis, the plates with the slide samples were transferred to a vacuum desiccator for 15-20 min until thawing. The analyses were performed on a Thermo Fisher Scientific Q Exactive Orbitrap MS (Thermo Scientific, San Jose, CA, USA) operating in the negative ion mode. DESI-MS images are created using a mobile station (2D moving stage Omni Spray, Prosolia Inc., Indianapolis, IN, USA) where samples are placed and directly scanned. The DESI probe remains stationary while the mobile station moves along the x and y directions. The x-axis represents the distance the mobile station covers at a constant speed, with the ionization source generating mass spectra at each point (pixel) during electrospray contact with the brain tissue. The y-axis consists of multiple lines with predefined spacing. Ultimately, the DESI probe scans the entire sample surface, capturing the spatial distribution of various analytes with high specificity. The brain tissues were scanned in horizontal rows (x-axis) separated by 150 to 300 µm vertical steps (y-axis). The lines were scanned at a constant velocity in the 170-280 µm s^{-1} range, and the mass spectra were recorded over the *m/z* 200-1000 range. Five micro scans were averaged, and the scan time was fixed at 0.7-1.4 s. Under these conditions, DESI-MS imaging experiments could achieve lateral spatial resolution in the 130-310 µm range. A sprayer-to-surface distance of 2 mm, a sprayer-to-MS inlet capillary distance of 5 mm, an incident spray angle of 54°, and a collection angle of 10° were used. The spray voltage was set at 5 kV. Nitrogen gas (160 psi) was used for nebulization. The spray solvent, acetonitrile (ACN) and *N*,*N*-dimethyl formaldehyde (DMF) in a proportion of 1:1 v v^{-1}, was sprayed on the brain tissue at a constant flow rate of 3.5 µL min^{-1}. Typical MS parameters included 5 micro scans, 100 ms maximum ion injection time, 15 V capillary voltage, 150 °C capillary temperature, 65 V tube lens voltage, 50 mu (manufacturer unit) S-lens RF level, 1250% automatic gain control (AGC), and 70000 resolution. These parameters resulted in between 2 and 5 spectra *per* s. All analyses were performed on the same day to avoid data inconsistency. The DESI-MS images were visually compared, with no statistical analysis performed. Specialized software is then employed to convert the mass spectra data into 2D spatially-resolved ion images. Each image illustrates the distribution of a specific ion on the surface, with the color scale indicating its intensity at a particular location. To handle and treat the MS data, the following software was used: (*i*) FireFly, 2.0.1 (Prosolia, Indianapolis, USA), for data translation into the acceptable format for graphical analysis, and (*ii*) BioMap 3x (Novartis Institute for Biomedical Research, Basel, Switzerland) for data visualization and interpretation.

Ion identification

The METLINTM (Metabolite and Chemical Entity Database) and LIPID MAPS (Lipid Metabolites and Pathways Strategy) databases identified all ions attributed to possible lipids detected in the mass spectra. In the METLINTM database, only those compounds with a maximum error of 1.5 ppm between the theoretical and experimental masses of the ions observed in the images were considered when assigning lipids categories. This parameter was set to give reliability to the results since no analytical standards were used to confirm the proposed species. Besides, the images generated from the ^{13}C-isotopologues were not considered. All proposed lipids were classified according to their category using the terminology and abbreviations established by the LIPID MAPS database. Figure 1 summarizes the entire experimental setup.

Results and Discussion

The following results pertain to the lipids identified in the negative ion mode. These lipids, typically identified in their deprotonated forms, exhibited significant changes in spatial distributions when exposed to gamma radiation. While lipids in the positive ion mode were also identified, a comparable behavior was not verified. The molecular formulae of the ions that effectively generated images (Figure 2) were proposed based on the high-resolution mass data (Table 1). Heavier isotopologues (with the ^{13}C isotope) were not included in the results (Figure 2 and Table 1) as they generated similar images to those of the lighter isotopologues. The METLINTM and LIPID MAPS databases were used to ascribe the classes to which each lipid belongs. These classes include fatty acids (FA), glycerophosphates (PA), glycerophospho-ethanolamines (PE), glycerophosphoglycerols (PG), glycerophosphoserines (PS), sphingolipids (SP), and glycerophosphoinositols (PI). No specific structures

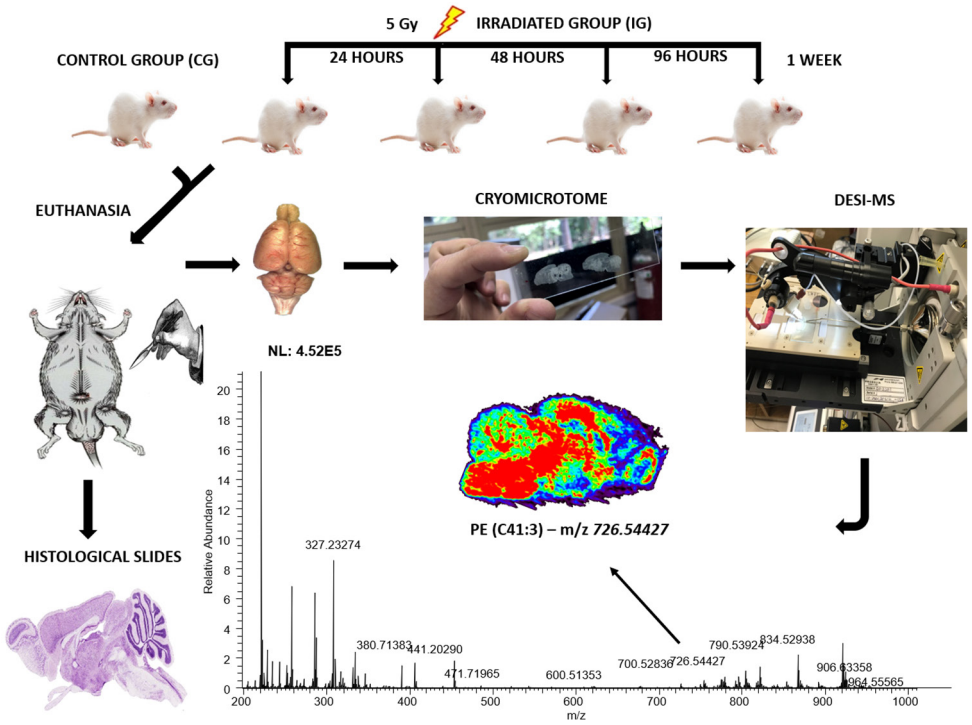

Figure 1. Graphical representation of the experimental flowchart up to attaining the DESI-MS images.

were suggested for these lipids due to the potential presence of multiple isomers for each formula. Some structures indicated by the database are unlikely to be detected by DESI-MS in the negative mode despite a negligible error between theoretical and experimental masses. Therefore, lipids from classes such as wax esters (WE), sterol lipids (ST), prenol lipids (PR), and glycerophosphocholines (PC) were excluded when assigning possible structures. The red color in the images of Figure 2 indicates the brain region with the highest intensity of a given ion. The color scales for the same lipid at different times after radiation exposure were standardized due to the absence of an internal standard. Figure 2 reveals that the ions dropped their intensity after 410 min of radiation exposure compared to the control samples. Subsequently, these intensities of the ions increased again, tending to return to the same levels as in the control samples (original condition). Certain lipid classes have already been identified and linked to various diseases. For instance, lipids from the FA class have been found in the serum and urine of individuals with schizophrenia[23] and are correlated with colorectal cancer (CRC).[24] Lipids from PG and PS classes have been observed in ductal fluid panels used for breast cancer diagnosis validation.[25] On the other hand, lipids from the PE class have been associated with the diagnosis of myeloid leukemia, hepatocellular carcinoma, genitourinary cancer, and lung carcinoma.[26-29]

Figure 3 displays various brain regions of Wistar rats, identified by numbers. Table 2 establishes the correlation between the occurrence of lipids (Figure 2, control group) and these specific brain regions.

The spatial distribution pattern reveals significant intensity differences between specific and adjacent regions for each lipid (Table 2). For instance, the ions of *m/z* 754.5752 (PE) and *m/z* 862.6069 (SP), though belonging to different classes, exhibit a notable similarity in spatial distribution, particularly in regions containing cerebellar fibers, tracts, and the brain stem. This suggests that these ions are constituents of these regions and may be linked to balance, motor skills, gait, delicate movements, and the coordination of motor automation execution. The ions of *m/z* 687.4966 (PA), 774.5442 (PE), 888.6237 (SP), and 857.5175 (PI) represent different lipid classes, yet they exhibit a distribution primarily covering the somatosensory regions and the hippocampus. Consequently, these ions in these regions may be linked to sensory perception processes, emotional modulation, and recent memory. The ions of *m/z* 774.5442 (PE), 797.5333 (PG), 834.5294 (PS), 857.5175 (PI), and 888.6237 (SP) belong to different classes and are distributed predominantly across the somatosensory regions, somatomotor, olfactory, frontal, and basal ganglia, collectively encompassing an extensive region known as the isocortex. This region, characterized by significant neuronal diversity, plays a crucial role in various functions, including sensory perceptions,

Table 1. Ion formula, experimental masses, mass errors, and the class assigned for the lipids detected in the brains of Winstar rats by MS in the negative ion mode

Ion formula	$[M - H]^-$ (*m/z*)	Error / ppm	Class
$C_{18}H_{33}O_2$	281.2484	1.23	FA (C18:1)
$C_{18}H_{35}O_2$	283.2640	0.93	FA (C18:0)
$C_{20}H_{31}O_2$	303.2328	1.20	FA (C20:4)
$C_{20}H_{37}O_2$	309.2797	0.99	FA (C20:1)
$C_{22}H_{35}O_2$	331.2640	1.01	FA (C22:4)
$C_{37}H_{70}O_8P$	673.4811	0.42	PA (C37:1)
$C_{38}H_{72}O_8P$	687.4966	0.19	PA (C38:1)
$C_{39}H_{75}NO_7P$	700.5284	0.35	PE (C39:1)
$C_{39}H_{75}NO_8P$	716.5240	1.28	PE (C39:1)
$C_{41}H_{73}NO_7P$	722.5128	0.44	PE (C41:5)
$C_{41}H_{77}NO_7P$	726.5443	0.70	PE (C41:3)
$C_{41}H_{79}NO_7P$	728.5595	0.13	PE (C41:2)
$C_{41}H_{73}NO_8P$	738.5078	0.50	PE (C41:4)
$C_{41}H_{79}NO_8P$	744.5544	0.15	PE (C41:1)
$C_{43}H_{73}NO_7P$	746.5132	1.02	PE (C43:6)
$C_{43}H_{77}NO_7P$	750.5439	0.22	PE (C43:4)
$C_{43}H_{81}NO_7P$	754.5752	0.18	PE (C43:2)
$C_{43}H_{73}NO_8P$	762.5077	0.42	PE (C43:6)
$C_{43}H_{75}NO_8P$	764.5226	–0.52	PE (C43:5)
$C_{43}H_{77}NO_8P$	766.5392	0.68	PE (C43:4)
$C_{45}H_{75}NO_7P$	772.5277	–0.49	PE (C45:7)
$C_{45}H_{77}NO_7P$	774.5442	0.55	PE (C45:6)
$C_{45}H_{81}NO_7P$	778.5750	–0.08	PE (C45:5)
$C_{42}H_{77}NO_{10}P$	786.5291	0.75	PS (C42:2)
$C_{45}H_{77}NO_8P$	790.5392	0.71	PE (C45:6)
$C_{44}H_{78}O_{10}P$	797.5333	0.05	PG (C44:4)
$C_{46}H_{77}NO_{10}P$	834.5294	1.04	PS (C46:6)
$C_{45}H_{78}O_{13}P$	857.5175	–0.59	PI (C45:4)
$C_{46}H_{88}NO_{11}S$	862.6069	–1.04	SP (C46:1)
$C_{47}H_{80}O_{13}P$	883.5338	0.12	PI (C47:5)
$C_{47}H_{82}O_{13}P$	885.5496	0.29	PI (C47:4)
$C_{48}H_{90}NO_{11}S$	888.6237	0.25	SP (C48:2)
$C_{49}H_{82}O_{13}P$	909.5496	0.33	PI (C49:6)

FA: fatty acid; PA: glycerophosphate; PS: glycerophosphoserine; PI: glycerophosphoinositol; PE: glycerophosphoethanolamine; PG: glycerophosphoglycerol; SP: sphingolipid.

behavior, olfactory perception, cognition and production, and the inhibitory control of voluntary/complex movements. The ions of *m/z* 303.2328 (FA), 309.2797 (FA), 687.4966 (PA), 774.5442 (PE), and 888.6237 (SP) exhibit spatial distribution in the hypothalamic region. This region plays a vital role in modulating eating behavior and energy expenditure. It can influence and modify the energy metabolism of various organs by responding to signals of peripheral nutrition and utilizing specialized sensors to control the overall energy balance.[31,32] FA or metabolites can signal nutritional sufficiency, decreasing glycogenolysis, gluconeogenesis, and liver lipogenesis. Consequently, the lipids identified in the hypothalamic region may indicate the pathophysiology associated with the development of obesity and metabolic syndrome (MetS).[33,34]

Ionizing radiation significantly induced changes in the lipidome, triggering a modulatory response that significantly altered spatial distribution and intensity of lipids. The images within the time kinetics reveal a pronounced decline within the initial 48 h across all regions. This suggests that each brain structure comprises multiple lipids, and the observed decrease may signify substantial neurophysiological changes with potential alterations in neurocognitive function, both in the short and/or long term. Metabolic response was observed after 96 h and one week, aiming to mitigate changes and restore physiological balance. However, even after one week, the spatial distribution of specific lipids, such as those of *m/z* 303.2328 (FA), 687.4966 (PA), 726.5443 (PE), and 862.6069 (SP), remains distinct from the control group. In contrast, other lipids, including those of *m/z* 673.4811 (PA), 754.5752 (PE), 797.5333 (PG), and 834.5294 (PS), exhibit a satisfactory response in minimizing the effects of ionizing radiation.

We have obtained unequivocal evidence demonstrating that ionizing radiation induces substantial alterations in the lipid profiles of animals exposed to radiation. This observation suggests a disturbance in synthesizing these lipids within the organism following radiation exposure. Notably, the individuals likely developed a regulatory mechanism to mitigate radiation-induced changes, although it remains uncertain whether permanent changes were triggered. The data obtained through DESI-MSI have provided valuable insights into understanding the lipidomic changes caused by radiation. To comprehend physiological and molecular mechanisms of radiation, conducting more comprehensive studies on its effects is imperative. Various potential avenues have been suggested, including direct DNA damage, the generation of ROS leading to the disruption of intermolecular DNA bonds, lipid oxidation, cellular and molecular repair signaling mechanisms, and intracellular microstructural changes.

Despite these unprecedented results, the present study presents some limitations. For example, no statistical analyses of the images were performed, and the results were based only on visual differences. Moreover, further investigations are required to unveil the impact of radiation exposure on other organs of the organism beyond the brain.

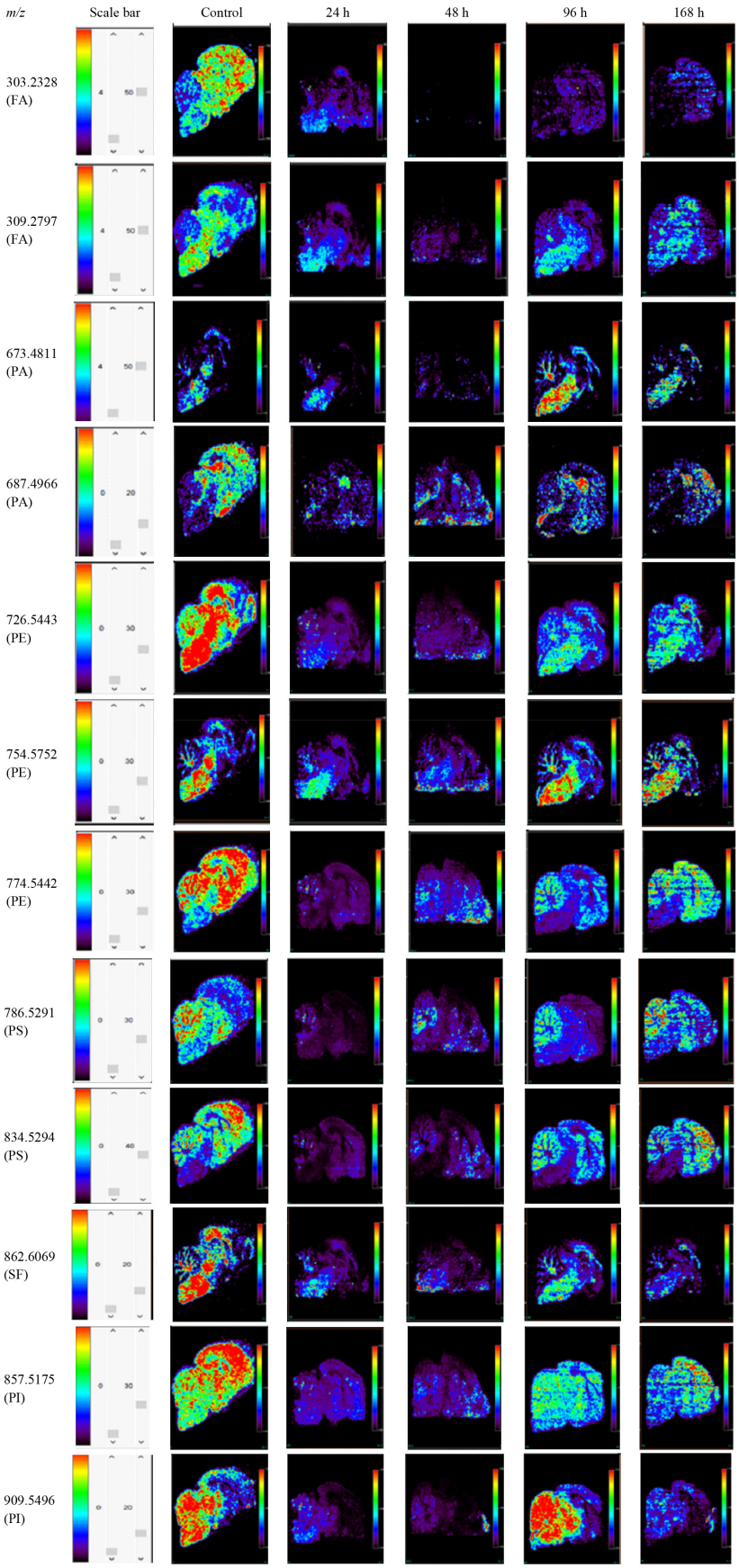

Figure 2. Spatial distribution of lipids in the Wistar rat brains as a function of exposure time to the gamma radiation.

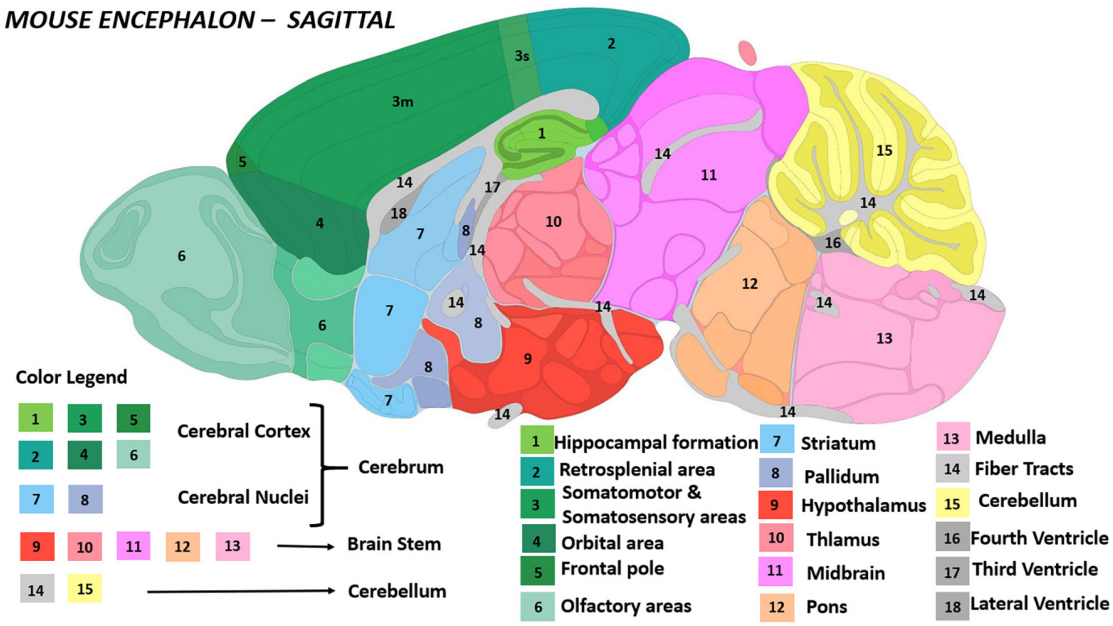

Figure 3. Diagram illustrating regions in the rat brain designated by both colors and numbers (adapted from reference 30).

Table 2. Occurrence of some lipids (as indicated in Table 1 and Figure 2, control group) in specific regions of Wistar rat brain

m/z (class)	Brain regions with high contents (red spots)
303.2328 (FA)	high intensity dispersed in the parenchyma in the regions (11), (1), (10), (2), (3), (4), (5), (6), (7), (8), and (9)
309.2797 (FA)	high intensity in the parenchyma of the brainstem regions (13), (12), (10), (11), and (9) with high density at the hypothalamus base; present in the regions (2), (3), (14) and in the fastigial nucleus of the cerebellum
673.4811 (PA)	high intensity in the parenchyma of the regions (12) and (11); the region (14) presents nerve fibers in the isocortex and cerebellar tracts
687.4966 (PA)	high intensity in the parenchyma of the regions (1), (10), (11), (2), and (3); focuses scattered on (9) and (12)
726.5443 (PE)	high density in the brainstem (11), (12), (13), (10), and (14), and tracts in the cerebral parenchyma: (3), (6), (7), (8); punctually present at the base of (9)
754.5752 (PE)	high intensity is mainly in (14) and the isocortex (between the hippocampus and somatomotor/sensory cortex); high intensity and density of points mainly in the brain stem: (11), (12), and (13)
774.5442 (PE)	high intensity diffusely throughout the cerebellar parenchyma, (1), (9), (10), (7), (8), (2), (3), (4), (5), (6); present in high density in the upper part of (11) and the lower part of the midbrain near the hypothalamus
786.5291 (PS)	high intensity diffusely spread throughout the (15) and (9) and present in the upper part of the (11); punctually in (13) and (3)
797.5333 (PG)	high intensity with great density in the parenchyma of the regions (7), (8), (10), (11), (2), (3), (4), (5), (9) and punctually in (15)
834.5294 (PS)	high intensity in the cerebral parenchyma: (1), (10), (3), (4), (5), (6), (7), (8); present with great density in the cerebellar leaves and upper midbrain; however, the pons, medulla, and lower midbrain have virtually no lipid intensity and density
857.5175 (PI)	high intensity with great density throughout (15), (1), (9), (10), (7), (8), (2), (3), (4), (5), and (6); high density in the upper part of (11) and regions of (12) and (13)
862.6069 (SP)	high intensity and density, mainly in (14) and fibers in the cerebellum and isocortex (between the hippocampus and somatomotor/sensory cortex); high intensity and density of points mainly in (10), (11), (12), and (13); regions with the highest density are (2), (3), and (6)
888.6237 (SP)	high intensity with great density, mainly in the regions of (14); great intensity and density of points mainly in the brain stem: (11), (12), and (13); regions with the highest density are (10), (11), (2), and (3); punctually in (6) and (7)
909.5496 (PI)	high intensity and density throughout cerebellar parenchyma (15), brainstem (11-midbrain; 12-bridge; 13-bulb), and part of thalamus (10); high density at the base of the hypothalamus (9)

FA: fatty acid; PA: glycerophosphate; PS: glycerophosphoserine; PI: glycerophosphoinositol; PE: glycerophosphoethanolamine; PG: glycerophosphoglycerol; SP: sphingolipid.

Conclusions

DESI-MSI facilitated the analysis of crucial lipid constituents in the Wistar rat brain, showcasing alterations in the primary cerebral lipid profiles resulting from radiation exposure. These lipid species exhibited distinct spatial distributions within the structures of the brain. Additionally, we investigated changes in spatial distribution over time kinetics, ranging from 24 to 168 h post-exposure to radiation. Gaining insight into the molecular response of brain tissue to radiation will enable a reassessment of planimetry and therapeutic protocols to minimize numerous undesirable neurocognitive effects, both in the short and long term.

Acknowledgments

The authors acknowledge the Brazilian agencies CNPq (National Council for Scientific Development), project REBRAT-SUS 456719, and CAPES (Coordination for the Improvement of Higher-Level Personnel) for the scholarships to Dr Matheus Soares Mingote. We thank Dr Luis Ladeira from CDTN (Nuclear Technology Development Center, LIG Laboratory) for the animal irradiation.

Author Contributions

Matheus F. S. Mingote was responsible for conceptualization, formal analysis, investigation, writing original draft; Camila Cristina A. de Paula for data curation, formal analysis, writing-review and editing; Tarcísio P. R. de Campos for conceptualization, formal analysis, project administration, resources; Géssica Adriana Vasconcelos for software, validation, visualization; Boniek G. Vaz for software, validation, visualization; Rodinei Augusti for data curation, formal analysis, writing-review and editing.

References

1. Miralbell, R.; Bleher, A.; Huguenin, P.; Ries, G.; Kann, R.; Mirimanoff, R.; Notter, M.; Nouet, P.; Bieri, S.; Thum, P.; Toussi, H.; *Int. J. Radiat. Oncol., Biol., Phys.* **1997**, *37*, 523. [Crossref]
2. Deb, P.; Fielding, A.; *Australasian Phys. Eng. Sci. Med.* **2009**, *32*, 51. [Crossref]
3. Goldwein, J. W.; Leahy, J. M.; Packer, R. J.; Sutton, L. N.; Curran, W. J.; Rorke, L. B.; Schut, L.; Littman, P.; D'Angio, G. J.; *Int. J. Radiat. Oncol., Biol., Phys.* **1990**, *19*, 1497. [Crossref]
4. Brown, P. D.; Buckner, J. C.; Uhm, J. H.; Shaw, E. G.; *Neuro-Oncology* **2003**, *5*, 161. [Crossref]
5. Brem, S. S.; Bierman, P. J.; Black, P.; Blumenthal, D.T.; Brem, H.; Chamberlain, M. C.; Chiocca, E. A.; DeAngelis, L. M.; Fenstermaker, R. A.; Fine, H. A.; Friedman, A.; Glass, J.; Grossman, S. A.; Heimberger, A. B.; Junck, L.; Levin, V.; Loeffler, J. J.; Maor, M. H.; Narayana, A.; Newton, H. B.; Olivi, A.; Portnow, J.; Prados, M.; Raizer, J. J.; Rosenfeld, S. S.; Shrieve, D. C.; Sills, A. K.; Spence, A. M.; Vrionis, F. D.; *J. Natl. Compr. Cancer Network* **2005**, *3*, 1540. [Crossref]
6. Alshykhly, O. R.; Fleming, A. M.; Burrows, C. J.; *Chem. Res. Toxicol.* **2015**, *28*, 1861. [Crossref]
7. Ackerstaff, E.; Glunde, K.; Bhujwalla, Z. M.; *J. Cell. Biochem.* **2003**, *90*, 525. [Crossref]
8. Peña-Bautista, C.; Vigor, C.; Galano, J.-M.; Oger, C.; Durand, T.; Ferrer, I.; Cuevas, A.; López-Cuevas, R.; Baquero, M.; López-Nogueroles, M.; Vento, M.; Hervás-Marín, D.; García-Blanco, A.; Cháfer-Pericás, C.; *Sci. Rep.* **2019**, *9*, 14244. [Crossref]
9. Han, X.; Gross, R. W.; *J. Lipid Res.* **2003**, *44*, 1071. [Crossref]
10. Han, X.; Jiang, X.; *Eur. J. Lipid Sci. Technol.* **2009**, *111*, 39. [Crossref]
11. Jung, H. R.; Sylvänne, T.; Koistinen, K. M.; Tarasov, K.; Kauhanen, D.; Ekroos, K.; *Biochim. Biophys. Acta, Spec. Sect. Lipids Relat. Subj.* **2011**, *1811*, 925. [Crossref]
12. Merrill, A. H.; Stokes, T. H.; Momin, A.; Park, H.; Portz, B. J.; Kelly, S.; Elaine, W.; Cameron, S. M.; Dongmei, W. M.; *J. Lipid Res.* **2009**, *50*, S97. [Crossref]
13. Lam, S. M.; Wang, Y.; Duan, X.; Wenk, M. R.; Kalaria, R. N.; Chen, C. P.; Lai, M. K. P.; Shui, G.; *Neurobiol. Aging* **2014**, *35*, 2369. [Crossref]
14. Takats, Z.; Wiseman, J. M.; Gologan, B.; Cooks, R. G.; *Science* **2004**, *306*, 471. [Crossref]
15. Cooks, R. G.; Ouyang, Z.; Takats, Z.; Wiseman, J. M.; *Science* **2006**, *311*, 1566. [Crossref]
16. Dill, A. L.; Ifa, D. R.; Manicke, N. E.; Ouyang, Z.; Cooks, R. G.; *J. Chromatogr. B* **2009**, *877*, 2883. [Crossref]
17. Eberlin, L. S.; Ferreira, C. R.; Dill, A. L.; Ifa, D. R.; Cooks, R. G.; *Biochim. Biophys. Acta, Spec. Sect. Lipids Relat. Subj.* **2011**, *1811*, 946. [Crossref]
18. Wu, C.; Dill, A. L.; Eberlin, L. S.; Cooks, R. G.; Ifa, D. R.; *Mass Spectrom. Rev.* **2013**, *32*, 218. [Crossref]
19. Cordeiro, F. B.; Jarmusch, A. K.; León, M.; Ferreira, C. R.; Pirro, V.; Eberlin, L. S.; Hallett, J.; Miglino, M. A.; Cooks, R. G.; *Anal. Bioanal. Chem.* **2020**, *412*, 1251. [Crossref]
20. Pirro, V.; Guffey, S. C.; Sepúlveda, M. S.; Mahapatra, C. T.; Ferreira, C. R.; Jarmusch, A. K.; Cooks, R. G.; *Mol. BioSyst.* **2016**, *12*, 2069. [Crossref]
21. Oliveira-Lima, O. C.; Carvalho-Tavares, J.; Rodrigues, M. F.; Gomez, M. V.; Oliveira, A.; Resende, R. R.; Gomez, R. S.; Vaz, B. G.; Pinto, M. C. X.; *Brain, Behav., Immun.* **2019**, *79*, 186. [Crossref]
22. Severiano, D. L.; Oliveira-Lima, O. C.; Vasconcelos, G. A.; Marques, B. L.; de Carvalho, G. A.; Freitas, E. M.; Xavier,

C. H.; Gomez, M. V.; Pinheiro, A. C. O.; Gomez, R. S.; Vaz, B. G.; Pinto, M. C. X.; *Neuroscience* **2020**, *426*, 1. [Crossref]
23. Yang, J.; Chen, T.; Sun, L.; Zhao, Z.; Qi, X.; Zhou, K.; Cao, Y.; Wang, X.; Qiu, Y.; Su, M.; *Mol. Psychiatry* **2013**, *18*, 67. [Crossref]
24. Brown, D. G.; Rao, S.; Weir, T. L.; O'Malia, J.; Bazan, M.; Brown, R. J.; Ryan, E. P.; *Cancer Metab.* **2016**, *4*, 11. [Crossref]
25. Matos do Canto, L.; Marian, C.; Varghese, R. S.; Ahn, J.; da Cunha, P. A.; Willey, S.; Sidawy, M.; Rone, J. D.; Cheema, A. K.; Luta, G.; *Int. J. Oncol.* **2016**, *49*, 2245. [Crossref]
26. Lin, L.; Huang, Z.; Gao, Y.; Chen, Y.; Hang, W.; Xing, J.; Yan, X.; *Proteomics* **2012**, *12*, 2238. [Crossref]
27. Nagai, K.; Uranbileg, B.; Chen, Z.; Fujioka, A.; Yamazaki, T.; Matsumoto, Y.; Tsukamoto, H.; Ikeda, H.; Yatomi, Y.; Chiba, H.; *Rapid Commun. Mass Spectrom.* **2020**, *34*, e8551. [Crossref]
28. Pabst, T.; Kortz, L.; Fiedler, G. M.; Ceglarek, U.; Idle, J. R.; Beyoğlu, D.; *BBA Clin.* **2017**, *7*, 105. [Crossref]
29. Wu, H.; Chen, Y.; Li, Z.; Liu, X.; *R. Soc. Open Sci.* **2018**, *5*, 181143. [Crossref]
30. Jones, A. R.; Overly, C. C.; Sunkin, S. M.; *Nat. Rev. Neurosci.* **2009**, *10*, 821. [Crossref]
31. Cone, R. D.; Cowley, M. A.; Butler, A. A.; Fan, W.; Marks, D. L.; Low, M. J.; *Int. J. Obes.* **2001**, *25*, S63. [Crossref]
32. Lenard, N. R.; Berthoud, H. R.; *Obesity* **2008**, *16*, S11. [Crossref]
33. Bruce, K. D.; Zsombok, A.; Eckel, R. H.; *Front. Endocrinol.* **2017**, *8*, 60. [Crossref]
34. de Morentin, P. B. M.; Varela, L.; Fernø, J.; Nogueiras, R.; Diéguez, C.; López, M.; *Biochim. Biophys. Acta, Spec. Sect. Lipids Relat. Subj.* **2010**, *1801*, 350. [Crossref]

Submitted: December 14, 2023
Published online: April 11, 2024